Available online at www.sciencedirect.com
SCIENCE DIRECT®
ELSEVIER
International Journal of Solids and Structures 41 (2004) 6895–6903
INTERNATIONAL JOURNAL OF SOLIDS and STRUCTURES
www.elsevier.com/locate/ijsolstr

Molecular assembly on cylindrical surfaces

W. Hong, Z. Suo *

Division of Engineering and Applied Sciences, Harvard University, Cambridge, MA 02138, USA

Received 22 December 2003; received in revised form 8 June 2004
Available online 17 July 2004

Abstract

A molecule adsorbed on a metal surface carries an electric dipole moment, and diffuses on the surface. When a collection of identical molecules partially covers the surface, the dipole–dipole interactions, along with other thermodynamic forces, drive the molecules to aggregate into monolayer islands, in the shape of dots or stripes. The dipole–dipole interactions mediate through the electrostatic field in the space. If the space is shaped, the electrostatic field will be affected, and so will the molecular pattern. To illustrate this idea, we develop a model to evolve molecular pattern on the surface of a wire, or the inner surface of a tube. Molecules assemble into parallel rings on the wire, and parallel stripes on the internal surface of a tube. When the tube radius is comparable to, or smaller than, the island size, the stripes switch to the rings; occasionally, the stripes form spirals.

Keywords: Self-assembly; Cylindrical surface; Phase pattern; Adsorbate

1. Introduction

Molecules and atoms absorbed on metallic surfaces carry electric dipoles (Evans and Ulman, 1990; Kellogg, 1994). The adsorbates can diffuse on the substrate surfaces (Barth, 2000). The dipole–dipole interaction, together with other inter-adsorbate forces, causes the adsorbates to self-assemble into a pattern, such as dots and stripes (Bohringer et al., 1999; Dmitriev et al., 2002; Xu et al., 2003). Similar patterns and analogous physics have been found in diverse systems, including lipid monolayers at the air/water interface (McConnell, 1991), block copolymer films (Harrison et al., 2000; Cheng et al., 2003), homopolymer films (Chou and Zhuang, 1999; Schaffer et al., 2000), ferrofluids (Dickstein et al., 1993), ferromagnets (De'Bell et al., 2000; Ifti et al., 2001), monolayer mixture on solid surfaces (Plass et al., 2001), and superconductors (Bianconi and Saini, 2001). Models of such phenomena have been reviewed by Seul and Andelman (1995), and Ng and Vanderbilt (1995).

When a system is isotropic, the self-assembled patterns lack long-range order. To break the symmetry, one can guide the adsorbate assembly with an external electric field (Gao and Suo, 2003; Suo and Hong,

* Corresponding author. Tel.: +1-617-4953789; fax: +1-617-4960601.
E-mail address: suo@deas.harvard.edu (Z. Suo).

0020-7683/$ - see front matter © 2004 Elsevier Ltd. All rights reserved.
doi:10.1016/j.ijsolstr.2004.06.014

2004). One can also break the symmetry in other ways. This article considers adsorbate assembly on cylindrical surfaces. To influence the adsorbate pattern, the cylinders should have radii comparable to the feature size of the adsorbate pattern. Technology now exists to manufacture wires and tubes of radii from micrometers to nanometers (Dong and Li, 2002). Adsorbates can self-assemble into patterns on the surface of a wire (a convex surface), or the inner surface of a tube (a concave surface). In both cases, the substrates are conductors. The two situations offer different spaces to mediate the dipole–dipole interaction, resulting in different adsorbate patterns. Following Suo et al. (2004), we will develop a phase field model to simulate adsorbate pattern evolution on cylindrical surfaces.

2. The model

Let (r, θ, z) be the cylindrical coordinates, and R be the radius of the cylindrical surface. The length of the cylinder is infinite. Let C be the adsorbate coverage, i.e., the fraction of surface sites occupied by the adsorbates. The coverage is restricted in the interval $0 < C < 1$. At time t, describe the adsorbate pattern on the cylindrical surface by the field $C(\theta, z, t)$. We do not consider the processes of adsorption and desorption. The cylindrical surface no longer exchanges molecules with the environment, so that the number of the adsorbates on the surface is time-independent. As the adsorbates diffuse on the surface, the pattern evolves, but the area-average coverage, C_0, is invariant.

The occupied and the vacant surface sites form a binary mixture, taken to obey the regular solution model. The free energy of mixing per unit surface area is

$$g(C) = \Lambda k_{\mathrm{B}} T[C \ln C + (1 - C) \ln(1 - C) + \Omega C(1 - C)], \tag{1}$$

where Λ is the number of surface sites per unit area, k_{B} Boltzmann's constant, and T the temperature. The first two terms in the bracket come from the entropy of mixing, and the third term from the enthalpy of mixing. The dimensionless parameter Ω measures the inter-adsorbate attraction relative to the thermal energy. When $\Omega < 2$, the thermal energy prevails, the function $g(C)$ has a single well, and the binary mixture forms a solution. When $\Omega > 2$, the inter-adsorbate attraction prevails, the function $g(C)$ has double wells, and the binary mixture separates into two phases.

The substrate is a conductor, and is submerged in a dielectric fluid of permittivity ε. The electric potential field in the dielectric, $\Psi(r, \theta, z, t)$, obeys the Laplace equation

$$\frac{\partial^2 \Psi}{\partial r^2} + \frac{\partial \Psi}{r \partial r} + \frac{\partial^2 \Psi}{r^2 \partial \theta^2} + \frac{\partial^2 \Psi}{\partial z^2} = 0. \tag{2}$$

The electric dipole moment of the adsorbates changes the contact potential of the substrate surface. We assume that the contact potential between the adsorbate-covered surface and the bare surface is proportional to the coverage. Let ζ be the contact potential between the fully covered surface and the bare surface. At a point approaching the surface, the electric potential in the dielectric equals the contact potential:

$$\Psi = \zeta C, r = R. \tag{3}$$

The contact potential prescribes the boundary condition to determine the electrostatic field in the dielectric.

The charge per unit area at the metal surface, $\sigma(\theta, z)$ is given by

$$\sigma = \pm \varepsilon \partial \Psi / \partial r, \quad r = R. \tag{4}$$

The positive sign is for the inner surface of a tube, and the negative sign is for the surface of a wire.

We adopt the approach of Cahn and Hilliard (1958), which, together with the time-dependent Ginzburg–Landau (TDGL) equation, has been widely used in the study of phase transition (Gunton et al., 1983). The coverage field obeys the diffusion equation (Suo et al., 2004):

$$\frac{\partial C}{\partial t} = \frac{M}{\Lambda^2}\nabla^2\left(\frac{\partial g}{\partial C} - 2h\nabla^2 C - \zeta\sigma\right). \tag{5}$$

Here M is the mobility of the adsorbate on the surface. The first term comes from the free energy of mixing, which accounts for the thermal energy and the inter-adsorbate interaction. The second term represents the gradient energy (Cahn and Hilliard, 1958), where h is a constant. The third term accounts for the dipole–dipole interaction. For adsorbates on cylindrical surfaces, the operator ∇^2 takes the form

$$\nabla^2 = \frac{\partial^2}{R^2\partial\theta^2} + \frac{\partial^2}{\partial z^2}. \tag{6}$$

The above model simultaneously evolves the coverage field $C(\theta, z, t)$ and the electric potential field $\Psi(r, \theta, z, t)$. At a given time, the coverage field is known. The electric potential field is determined by solving the boundary value problem. The resulting surface charge density enters the right-hand side of Eq. (5), which updates the coverage field for a small time step. Repeat this procedure for many time steps, and one evolves the two fields over a long time.

3. Electrostatic field in the Fourier space

The electric potential field is subject to the boundary condition (3), which is nonuniform. The boundary value problem can be solved analytically in the Fourier space. Transform only the two surface coordinates of any given function, for example,

$$\Psi(r, \theta, z, t) = \sum_{m=-\infty}^{\infty}\int_{-\infty}^{\infty}\widehat{\Psi}_{mn}(r, t)\exp(im\theta + inz)\mathrm{d}n, \tag{7}$$

where m is an integer, n the wave number in the axial direction, and $\widehat{\Psi}_{mn}$ the Fourier component. The Laplace equation (2) becomes an ordinary differential equation for the function $\widehat{\Psi}_{mn}(r, t)$:

$$\frac{d^2\widehat{\Psi}_{mn}}{dr^2} + \frac{d\Psi_{mn}}{rdr} - \left(n^2 + \frac{m^2}{r^2}\right)\widehat{\Psi}_{mn} = 0. \tag{8}$$

In the Fourier space, the boundary condition (3) becomes $\widehat{\Psi}_{mn}(R, t) = \zeta\widehat{C}_{mn}(t)$.

When $n = 0$, the solution to the boundary value problem is

$$\widehat{\Psi}_{m0}(r, t) = \zeta\widehat{C}_{m0}(t)(r/R)^{\pm m}. \tag{9}$$

The positive sign is for the field inside a tube, and the negative sign is for the field surrounding a wire. The surface charge density is

$$\hat{\sigma}_{m0}(t) = m\varepsilon\zeta\widehat{C}_{m0}(t)/R. \tag{10}$$

When $n \neq 0$, on dividing Eq. (8) by n^2, one confirms that the solution is a function of nr. Eq. (8) becomes Bessel's modified differential equation (Abramowitz and Stegun, 1964). The general solution is a linear combination of $I_m(nr)$ and $K_m(nr)$, the modified Bessel function of the first and the second kind of order m. The function $I_m(nr)$ is well-behaved for $0 \leqslant r < \infty$, but is unbounded as $r \to \infty$. The function $K_m(nr)$ is well-behaved for $0 < r < \infty$, vanishes as $r \to \infty$, but is unbounded as $r \to 0$.

The electric potential field outside a wire is

$$\widehat{\Psi}_{mn}(r, t) = \zeta\widehat{C}_{mn}(t)K_m(nr)/K_m(nR). \tag{11}$$

The potential field matches the contact potential on the wire surface, and vanishes as $r \to \infty$. Inserting this potential field into Eq. (4), we obtain the charge density on the wire surface:

$$\hat{\sigma}_{mn}(t) = \varepsilon\zeta\widehat{C}_{mn}(t)\left[n\frac{K_{m+1}(nR)}{K_m(nR)} - \frac{m}{R}\right]. \tag{12}$$

The electric potential field inside a tube is

$$\widehat{\Psi}_{mn}(r,t) = \zeta\widehat{C}_{mn}(t)I_m(nr)/I_m(nR). \tag{13}$$

The potential field matches the contact potential on the inner surface of the tube, and remains bounded everywhere inside the tube. Inserting this potential field into Eq. (4), we obtain the charge density on the inner surface of the tube:

$$\hat{\sigma}_{mn}(t) = \varepsilon\zeta\widehat{C}_{mn}(t)\left[n\frac{I_{m+1}(nR)}{I_m(nR)} + \frac{m}{R}\right]. \tag{14}$$

4. Numerical method

A comparison of the first two terms in the parenthesis in Eq. (5) defines a length:

$$b = \left(\frac{h}{\Lambda k_{\mathrm{B}}T}\right)^{1/2}. \tag{15}$$

In the Cahn–Hilliard model, this length scales the distance over which the coverage changes from the level of one phase to that of the other. One may consider b the width of the phase boundary.

From Eq. (5), disregarding a dimensionless factor, we note that the diffusivity scales as $D \sim Mk_{\mathrm{B}}T/\Lambda$. To resolve events occurring over the length scale of the phase boundary width, b, the time scale is $\tau = b^2/D$, namely,

$$\tau = \frac{h}{M(k_{\mathrm{B}}T)^2}. \tag{16}$$

In Eq. (5), we normalize the spatial coordinates by b, the time by τ, and the energy by $k_{\mathrm{B}}T$. A dimensionless number,

$$W = \frac{\varepsilon\zeta^2}{\sqrt{h\Lambda k_{\mathrm{B}}T}}, \tag{17}$$

appears in the normalized equation. The number W represents the magnitude of the molecular dipole moment relative to the intermolecular attraction.

On the surface of a wire, the adsorbate pattern evolves according to

$$\frac{\partial\widehat{C}_{mn}}{\partial\hat{t}} = -k^2\widehat{P}_{mn} - 2k^4\widehat{C}_{mn} + Wk^2\widehat{C}_{mn}\left[n\frac{K_{m+1}(nR)}{K_m(nR)} - \frac{m}{R}\right]. \tag{18}$$

On the inner surface of a tube, the adsorbate pattern evolves according to

$$\frac{\partial\widehat{C}_{mn}}{\partial\hat{t}} = -k^2\widehat{P}_{mn} - 2k^4\widehat{C}_{mn} + Wk^2\widehat{C}_{mn}\left[n\frac{I_{m+1}(nR)}{I_m(nR)} + \frac{m}{R}\right]. \tag{19}$$

In Eq. (18) and (19), R and n are normalized by b, the wave number is $k = \sqrt{(m/R)^2 + n^2}$, and $\widehat{P}_{mn}$ is a Fourier component of the function

$$P(\theta,z,t) = \ln\left(\frac{C}{1-C}\right) + \Omega(1-2C). \tag{20}$$

When the radius of the cylinder, R, is much larger than b, both Eq. (18) and (19) recover the equation for adsorbates on a flat surface derived by Suo et al. (2004).

We adapt the numerical method in Lu and Suo (2001) for this problem. To make the calculation finite, we apply the periodic boundary condition in the axial direction, and perform calculation in one period. In presenting the simulation result, we spread the cylindrical surface into a flat rectangle. One should mentally connect the left and right borders to form a full circumference. Divide the rectangle into square grids, with the grid size $0.5b$ in both axial and circumferential directions. The rectangle has 256 grids in the axial direction. We use the values of the cylinder radius to ensure integer numbers of grids in the circumferential direction. We visualize the adsorbate pattern by plotting the coverage field in the rectangular cell using a gray scale.

Eq. (18) and (19) have to be integrated over a long time to reach the equilibrium adsorbate pattern. To maintain stability, we adopt the semi-implicit method proposed by Chen and Shen (1998). At each time step, the P field is calculated from the C field on every grid point according to Eq. (20). Both fields are transformed into $\widehat{P}$ and $\widehat{C}$ in Fourier space. Eq. (18) or (19) updates $\widehat{C}$ for the next time step. Transform the updated $\widehat{C}$ back to the real space. The procedure is repeated for every time step. We use the fast Fourier transformation. The modified Bessel functions are evaluated using the polynomial coefficients given in Abramowitz and Stegun (1964).

5. Simulation results

The balance between coarsening and refining sets the phase size. This balance is controlled through the dimensionless number W, which is set to be $W = 2$. We take $\Omega = 2.2$ in the simulation, so that the free energy of mixing, $g(C)$, has two wells at the coverage 0.25 and 0.75. At time $t = 0$, we introduce some randomness by prescribing the coverage at the every grid point within 0.001 from the average coverage. Unless otherwise stated, we will present snapshots taken at the time $t = 10000\tau$.

Fig. 1 shows a time sequence of adsorbate patterns on a wire of radius $R = 10.19b$. The average coverage is $C_0 = 0.5$. The adsorbates quickly form a two-phase mixture, which assemble into stripes. Initially, the stripes are thin and randomly oriented. As the time goes on, the strips coarsen and straighten, aligned in the direction perpendicular to the axis of the wire. As a compromise between the gradient energy and electrostatic energy, the stripe width approaches an equilibrium value. Afterwards, the topology of the strip pattern changes slowly: defects in the strip connections remain after an extremely long time.

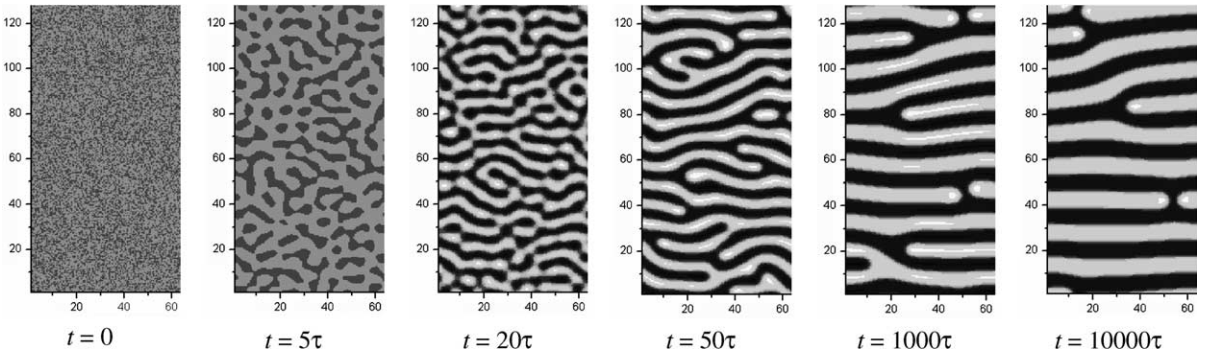

Fig. 1. A time sequence of adsorbate patterns evolving on a wire of radius $R = 10.19b$. The cylindrical surface is spread into a rectangle in the plane, with the circumference direction in the horizontal direction. The average coverage is $C_0 = 0.5$. As time goes on, the adsorbates separate into two phases. Stripes emerge, coarsen, straighten, and align along the circumference of the wire.

On the wire surface, the adsorbate stripes prefer to align along the circumference, rather than along the cylinder axis. This can be understood in terms of the electrostatic energy. The electrostatic field in the space surrounding the wire results from the contact potential between the stripes of the two phases. The stripes act like electrodes. When the effective distance between the electrodes is small, the capacitance is large, and therefore the electrostatic free energy is small. On the wire surface, the circumferential stripes have a smaller effective distance than the axial stripes. Consequently, the former is preferred.

Fig. 2 shows the snapshots of the adsorbate pattern on wires of several radii. The average coverage is $C_0 = 0.5$. The smaller the wire radius, the better the adsorbate stripes are aligned. When the radius is small enough, every stripe is connected to itself, forming a ring around the wire. All the rings form a periodic array. When the wire radius is comparable to the intrinsic length b, the equilibrium stripe width reduces significantly.

Fig. 3 shows the snapshots of the adsorbate pattern on wires of several radii. The average coverage is $C_0 = 0.4$. When the wire radius is large, the adsorbates at the average coverage 0.4 form dots, just like the adsorbate patterns formed on a flat surface (Suo et al., 2004). However, the dots formed on the wire tend to elongate in the circumferential direction. When the wire is thin enough, each single dot becomes so elongated that it forms a ring around the wire. All the rings form a periodic array.

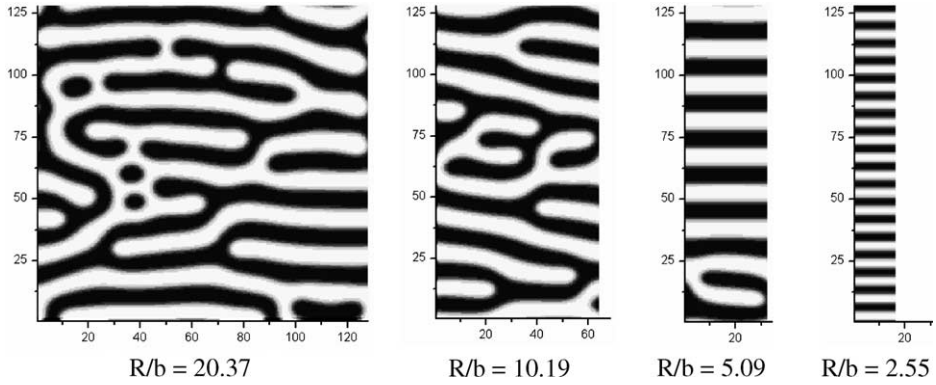

Fig. 2. Snapshots of adsorbate patterns on wires of several radii. The average coverage is $C_0 = 0.5$. The thinner the wire, the thinner the stripes, and the better they align.

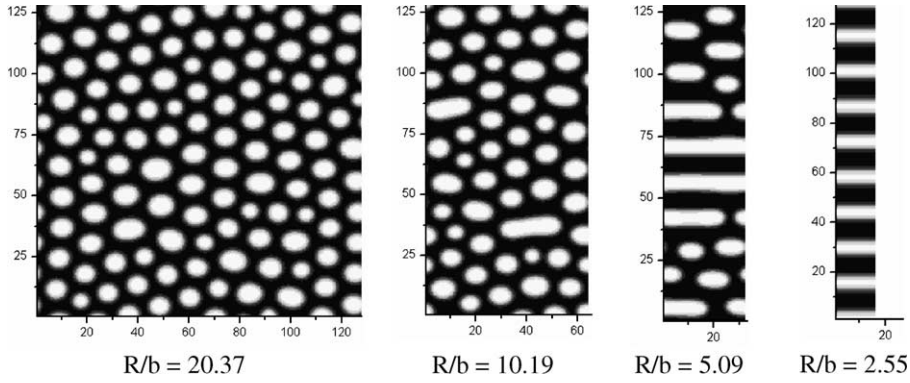

Fig. 3. Snapshots of adsorbate patterns on wires of several radii. The average coverage is $C_0 = 0.4$. For a thick wire, the adsorbates form dots. For a thin wire, the dots elongate. For a very thin wire, each dot is so elongated that it forms a ring around the wire.

We next consider adsorbate patterns on the inner surface of a tube. In the space inside the tube, the axial stripes have a smaller effective distance than the circumferential stripes. Consequently, we expect the adsorbate stripes to align along the tube axis. Fig. 4 shows the snapshots of the adsorbate patterns on the internal surfaces of tubes of several radii. The average coverage is $C_0 = 0.5$. When R/b is large, the stripes indeed tend to align along the tube axis. When the tube is thinner, the stripes also become thinner. When the tube becomes too thin, the space is too crowded to accommodate the axial stripes, and adsorbates form rings instead. However, our simulation shows that such rings will keep coarsening. For some intermediate tube radii, we find that the stripes are at an angle from the tube radius, forming spirals.

Fig. 5 shows the snapshots of the adsorbate patterns on the internal surfaces of tubes of several radii. The average coverage is $C_0 = 0.4$. When the tube radius is large, the adsorbates form dots similar to those on a flat substrate. As the tube radius decreases, the dots elongate along the tube axis, and possibly become axial stripes. For very thin tubes, the space shortage forces the adsorbates to form rings around the tube.

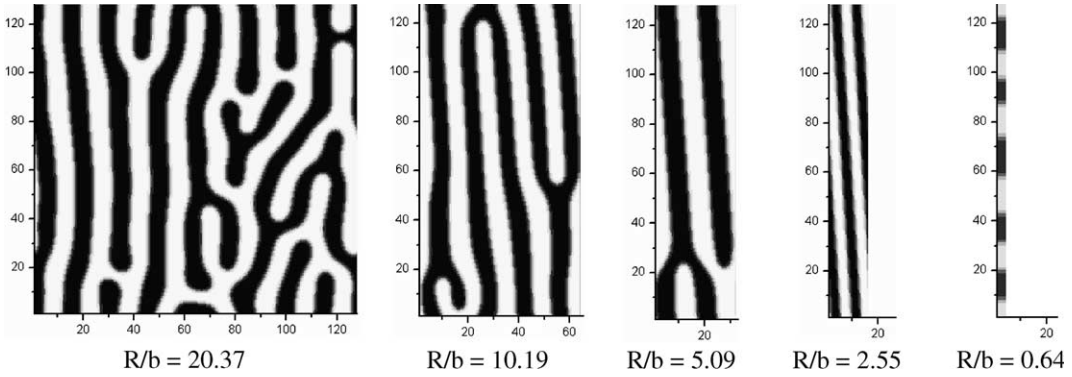

Fig. 4. Snapshots of adsorbate patterns on the inner surface of tubes of several radii. The average coverage is $C_0 = 0.5$. For a thick tube, the stripes align along the tube axis. As the tube radius decreases, the space shortage first forces the stripes into spirals, and finally into rings.

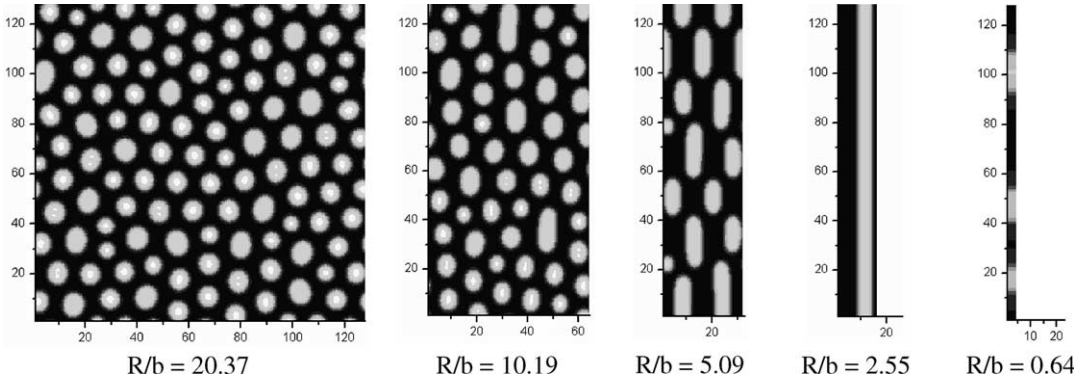

Fig. 5. Snapshots of adsorbate patterns on the inner surface of tubes of several radii. The average coverage is $C_0 = 0.4$. As the tube radius decreases, the dots first elongate along the tube axis, then become axial stripes, and finally switch to rings.

6. Concluding remarks

Molecules adsorbed on a solid surface are mobile electric dipoles. The thermal energy motivates the adsorbate to disperse evenly on the surface, and the inter-adsorbate attraction motivates the adsorbates to form monolayer aggregates. When the adsorbates do form aggregates, the dipole–dipole interaction limits the aggregate size. This paper studies adsorbate pattern evolution on the surfaces of wires and tubes. The cylindrical geometry breaks the symmetry of the space, guiding the aggregates to align in preferred directions. The tubes and wires offer different space to mediate the dipole–dipole interaction, so that adsorbates form dissimilar patterns on two types of surfaces. When the wires or the tubes are very thin, the space shortage in the circumferential direction forces the adsorbates to change patterns. Technology now exists to produce wires and tubes of radius from micrometers to nanometers. We eagerly await experimental demonstrations of molecular assembly on surfaces of the wires and tubes.

Acknowledgements

This work has been supported by DOE through grant DE-FG02-03ER46091, and by the Division of Engineering and Applied Sciences at Harvard University.

References

Abramowitz, M., Stegun, I.A., 1964. Handbook of Mathematical Functions. Reprinted by Dover Publications Inc., New York.
Barth, J.V., 2000. Transport of adsorbates at metal surfaces: from thermal migration to hot precursors. Surf. Sci. Rep. 40, 75–149.
Bianconi, A., Saini, N.L., 2001. Stripes and Related Phenomena. Kluwer.
Bohringer, M., Morgenstern, K., Schneider, W.D., Berndt, R., Mauri, F., De Vita, A., Car, R., 1999. Two-dimensional self-assembly of supramolecular clusters and chains. Phys. Rev. Lett. 83, 324–327.
Cahn, J.W., Hilliard, J.E., 1958. Free energy of a nonuniform system. I. interfacial free energy. J. Chem. Phys. 28, 258–267.
Chen, L.Q., Shen, J., 1998. Applications of semi-implicit Fourier-spectral method to phase field equations. Comput. Phys. Commun. 108, 147–158.
Cheng, J.Y., Ross, C.A., Thomas, E.L., Smith, H.I., Vancso, G.J., 2003. Templated self-assembly of block copolymers: Effect of substrate topography. Adv. Mater. 15, 1599–1602.
Chou, S.Y., Zhuang, L.J., 1999. Lithographically induced self-assembly of periodic polymer micropillar arrays. Vac. Sci. Technol., B 17, 3197–3202.
De'Bell, K., Maclsaac, A.B., Whitehead, J.P., 2000. Dipolar effects in magnetic thin films and quasi-two-dimensional systems. Rev. Mod. Phys. 72, 225–257.
Dickstein, A.J., Erramilli, S., Goldstein, R.E., Jackson, D.P., Langer, S.A., 1993. Labyrinthine pattern-formation in magnetic fluids. Science 261, 1012–1015.
Dmitriev, A., Lin, N., Weckesser, J., Barth, J.V., Kern, K., 2002. Supramolecular assemblies of trimesic acid on a Cu (1 0 0) surface. J. Phys. Chem. B. 106, 6907–6912.
Dong, Y.J., Li, Y.D., 2002. Synthesis, assembly and device of 1-dimensional nanostructures. Chin. Sci. Bull. 47, 1149–1156.
Evans, S.D., Ulman, A., 1990. Surface-potential studies of alkyl-thiol monolayers adsorbed on gold. Chem. Phys. Lett. 170, 462–466.
Gao, Y.F., Suo, Z., 2003. Guided self-assembly of molecular dipoles on a substrate surface. J. Appl. Phys. 93, 4276–4282.
Gunton, J.D., San Miguel, M., Sahni, P.S., 1983. In: Domb, C., Lebowitz, J.L. (Eds.), Phase Transitions and Critical Phenomena, Vol. 8. Academic.
Harrison, C., Adamson, D.H., Cheng, Z.D., Sebastian, J.M., Sethuraman, S., Huse, D.A., Register, R.A., Chaikin, P.M., 2000. Mechanisms of ordering in striped patterns. Science 290, 1558–1560.
Ifti, M., Li, Q., Soukoulis, C.M., Velgakis, M.J., 2001. A study of 2D Ising ferromagnets with dipole interactions. Mod. Phys. Lett. B, 15895–15903.
Kellogg, G.L., 1994. Field-ion microscope studies of single-atom surface-diffusion and cluster nucleation on metal-surfaces. Surf. Sci. Rep. 21, 1–88.
Lu, W., Suo, Z., 2001. Dynamics of nanoscale pattern formation of an epitaxial monolayer. J. Mech. Phys. Solids 49, 1937–1950.
McConnell, H.M., 1991. Structures and transitions in lipid monolayers at the air-water interface. Annu. Rev. Phys. Chem. 42, 171–195.

Ng, K.-O., Vanderbilt, D., 1995. Stability of periodic domain-structures in a 2-dimensional dipolar model. Phys. Rev. B 52, 2177–2183.
Plass, R., Last, J.A., Bartelt, N.C., Kellogg, G.L., 2001. Nanostructures—self-assembled domain patterns. Nature 412, 875–875.
Schaffer, E., Thurn-Albrecht, T., Russell, T.P., Steiner, U., 2000. Electrically induced structure formation and pattern transfer. Nature 403, 874–877.
Seul, M., Andelman, D., 1995. Domain shapes and patterns—the phenomenology of modulated phases. Science 267, 476–483.
Suo, Z., Hong, W., 2004. Programmable motion and assembly of molecules on solid surfaces. Proc. Nat. Acad. Sci. 101, 7874–7879.
Suo, Z., Gao, Y.F., Scoles, G., 2004. Nanoscale domain stability in organic monolayers on metals. J. Appl. Mech. 71, 24–31.
Xu, F.T., Street, S.C., Barnard, J.A., 2003. Coverage dependent evolution of two-dimensional dendrimer/mica domain pattern. J. Phys. Chem. B 107, 12762–12767.